



HAL
open science

Interaction network among de novo purine nucleotide biosynthesis enzymes in *Escherichia coli*

Antoine Gedeon, Gouzel Karimova, Nour Ayoub, Julien Dairou, Quentin Gai Gianetto, Sophie Vichier-Guerre, Pierre-olivier Vidalain, Daniel Ladant, Hélène Munier-lehmann

► To cite this version:

Antoine Gedeon, Gouzel Karimova, Nour Ayoub, Julien Dairou, Quentin Gai Gianetto, et al.. Interaction network among de novo purine nucleotide biosynthesis enzymes in *Escherichia coli*. *FEBS Journal*, 2023, 290, pp.3165-3184. 10.1111/febs.16746 . pasteur-04092979

HAL Id: pasteur-04092979

<https://pasteur.hal.science/pasteur-04092979v1>

Submitted on 9 May 2023



HAL is a multi-disciplinary open access archive for the deposit and dissemination of scientific research documents, whether they are published or not. The documents may come from teaching and research institutions in France or abroad, or from public or private research centers.

L'archive ouverte pluridisciplinaire **HAL**, est destinée au dépôt et à la diffusion de documents scientifiques de niveau recherche, publiés ou non, émanant des établissements d'enseignement et de recherche français ou étrangers, des laboratoires publics ou privés.



Distributed under a Creative Commons Attribution - NonCommercial - NoDerivatives 4.0 International License

Interaction network among *de novo* purine nucleotide biosynthesis enzymes in *Escherichia coli*

Antoine Gedeon^{1,2,*} , Gouzel Karimova^{1,3}, Nour Ayoub^{1,2,†}, Julien Dairou⁴, Quentin Gai Gianetto^{1,5}, Sophie Vichier-Guerre^{1,6}, Pierre-Olivier Vidalain^{4,7}, Daniel Ladant^{1,3} and H el ene Munier-Lehmann^{1,2,†} 

1 Institut Pasteur, Universit  Paris Cit , Paris, France

2 Unit  de Chimie et Biocatalyse, CNRS UMR3523, Paris, France

3 Unit  de Biochimie des Interactions Macromol culaires, CNRS UMR3528, Paris, France

4 Laboratoire de Chimie et Biochimie Pharmacologiques et Toxicologiques, Universit  Paris Cit , Paris, France

5 Plateforme Prot omique, Unit  de Technologie et Service Spectrom trie de Masse pour la Biologie, CNRS UAR 2024 & Hub de Bioinformatique et Biostatistiques, Paris, France

6 Unit  Chimie Biologique Epig n tique, CNRS UMR3523, Paris, France

7 Team VIRIMI, CIRI, Univ Lyon, INSERM U1111, Universit  Claude Bernard Lyon 1, CNRS UMR5308, ENS de Lyon, Lyon, France

Keywords

bacterial two-hybrid system; *de novo* purine biosynthesis; *Escherichia coli*; supramolecular assembly

Correspondence

D. Ladant, Institut Pasteur, Unit  de Biochimie des Interactions Macromol culaires, 28 rue du Dr Roux, 75015 Paris, France

Tel.: 33-1-45-68-84-00

E-mail: daniel.ladant@pasteur.fr

H. Munier-Lehmann, Institut Pasteur, Unit  de Chimie et Biocatalyse, 28 rue du Dr Roux, 75015 Paris, France

Tel.: 33-1-45-68-83-81

E-mail: helene.munier-lehmann@pasteur.fr

Present address

^{*}Unit  de Microbiologie Structurale, Institut Pasteur, Universit  Paris Cit , CNRS UMR3528, France

[†]Plateforme Criblage Ch mog nomique et Biologique, Institut Pasteur, Universit  Paris Cit , CNRS UMR3523, France

In human cells, *de novo* purine nucleotide biosynthesis is known to be regulated through the formation of a metabolon called purinosome. Here, we employed a bacterial two-hybrid approach to characterize the protein–protein interactions network among the corresponding enzymes of *Escherichia coli*. Our study revealed a dense network of binary interactions that connect most purine nucleotide biosynthesis enzymes. Notably, PurK, an exclusive prokaryotic enzyme, appears as one of the central hubs of this network. We further showed that modifications in PurK, which disrupted several interactions in the network, affected the purine nucleotide pools and altered the bacterial fitness. Our data suggest that the bacterial *de novo* purine nucleotide biosynthesis enzymes can assemble in a supramolecular complex and that proper interactions among the components of this complex can contribute to bacterial fitness.

Abbreviations

AdS, adenylosuccinate; AICAR, 5-aminoimidazole-4-carboxamide ribonucleotide; AIR, 5-aminoimidazole ribonucleotide; AM(D/T)P, adenosine 5'-mono(di/tri)phosphate; BACTH, bacterial two-hybrid system; CAIR, 5-phosphoribosyl-4-carboxy-5-aminoimidazole; cAMP, cyclic AMP; FAICAR, 5-formamidoimidazole-4-carboxamide ribonucleotide; FGAM, 5'-phosphoribosyl-N-formyl glycineamide; FGAR, 5'-phosphoribosyl-N-formylglycinamide; FH₄, tetrahydrofolic acid; GAR, 5'-phosphoribosylglycinamide; GM(D/T)P, guanosine 5'-mono(di/tri)phosphate; Icd, isocitrate dehydrogenase; IMP, inosine 5'-monophosphate; NAD⁺/NADH, nicotinamide adenine dinucleotide; NCAIR, N5-carboxyamino-imidazole ribonucleotide; ORFs, open reading frames; PRA, 5-phosphoribosyl-1-amine; PRPP, 5-phosphoribosyl-1-pyrophosphate; R₅P, ribose 5-phosphate; SAICAR, 5-Amino-4-imidazole-N-succinocarboxamide ribonucleotide; TCA, tricarboxylic acid cycle; XMP, xanthosine 5'-monophosphate.

Gouzel Karimova and Nour Ayoub
contributed equally to this article

(Received 12 September 2022, revised 10
January 2023, accepted 6 February 2023)

doi:10.1111/febs.16746

Introduction

Metabolic pathways are formed of multiple reactions catalysed by enzymes that produce or breakdown biomolecules. Several modes of regulation take place to maintain *ad hoc* concentrations of metabolites in cells. In 1985, P.A. Srere proposed the word metabolon to describe a «supramolecular complex of sequential metabolic enzymes and cellular structural elements» [1]. Physical proximity of the enzymes involved in a given metabolic pathway may favour substrate channelling and therefore optimize metabolic flux [2]. Since then, the concept of metabolon has been extended to other metabolic pathways in bacteria and plants [3,4]. Above all, glycolysis [5–8], cyanogenic glucoside synthesis [9], folate metabolism [10], branched-chain amino acids synthesis [11], ubiquinone synthesis [12] and *de novo* purine nucleotide biosynthesis [13–16] were proposed to be regulated via metabolon formation.

De novo purine nucleotide biosynthesis is one of two possible routes to produce adenine and guanine nucleotides, the other being the salvage pathway. The salvage pathway is sufficient to maintain the purine nucleotide pool in standard physiological conditions, whereas the *de novo* pathway is upregulated in highly demanding conditions, such as DNA replication and cell division. The chemical steps of the *de novo* pathway (Fig. 1) are evolutionarily conserved in all living organisms [17]. Phosphoribosylpyrophosphate (PRPP) is first converted via 10 steps into the intermediate nucleotide inosine 5'-monophosphate (IMP). At this branching point, IMP is subsequently converted into AMP or GMP via two separate routes, each formed of two distinct steps. In mammalian cells, nine enzymes are implicated in *de novo* synthesis [18], with several multifunctional, including one trifunctional enzyme (TrifGART) and three bifunctional enzymes (PAICS, ATIC, ADSL). Conversely, 14 enzymes have been identified in prokaryotes [19] with only two bifunctional enzymes, PurB and PurH (ADSL and ATIC homologues respectively). Additionally, two possible routes catalyse the third step in bacteria, one supported by the folate-dependent PurN (the equivalent of the GAR Tfase domain of mammalian TrifGART), and the other by the formate-dependent prokaryote-specific PurT. Another difference encountered in

prokaryotes concerns the sixth step: it is split into two sequential reactions, the first one catalysed by PurK, an enzyme that has no eukaryotic homologue, and the second one catalysed by PurE, the equivalent of the CAIR synthetase domain of PAICS.

In human cells, the *de novo* purine nucleotide biosynthetic pathway has long been proposed to form a metabolon. Benkovic's team first reported in 2008 a co-localization of all the enzymes involved in the first 10 reactions of the pathway and proposed that these enzymes could assemble into a supramolecular complex, called purinosome, in purine-depleted conditions [15]. In 2015, two other enzymes from the pathway (IMPDH and ADSS, see Fig. 1) were also grouped into the megacomplex [20]. Purinosome formation was shown to be regulated by various environmental factors and signalling pathways (e.g. purine-depletion, hypoxic growth conditions) with a dynamic assembly and disassembly pattern [21–24]. Recently, a link between purinosome formation and an increase in purine nucleotide synthesis has been shown by metabolomics and mass spectrometry imaging [25].

Whether a *de novo* purine nucleotide biosynthetic metabolon also exists in prokaryotes has long been speculative [26]. Former studies on two *E. coli* enzymes of this pathway have revealed transient interaction channelling via kinetic analysis [27]. Here, we have considered all enzymes belonging to the *de novo* purine nucleotide biosynthesis, including those after the IMP branching point (Fig. 1). By using a bacterial adenylate cyclase two-hybrid (BACTH) approach, we characterized the protein–protein interaction network among all these enzymes and provided experimental evidence suggesting the existence of a multi-molecular complex in *E. coli*. Interestingly, we identified the bacterial-specific enzyme, namely PurK, as one of the central connectors. We further showed that PurK modifications that disrupt its association with several *de novo* purine nucleotide biosynthesis enzymes, directly affected the adenine and guanine nucleotide pools and impacted the bacterial fitness. Hence, these data strongly support the hypothesis that proper associations between the *de novo* purine nucleotide biosynthesis enzymes provide a growth advantage to *E. coli* when this pathway is essential for survival.

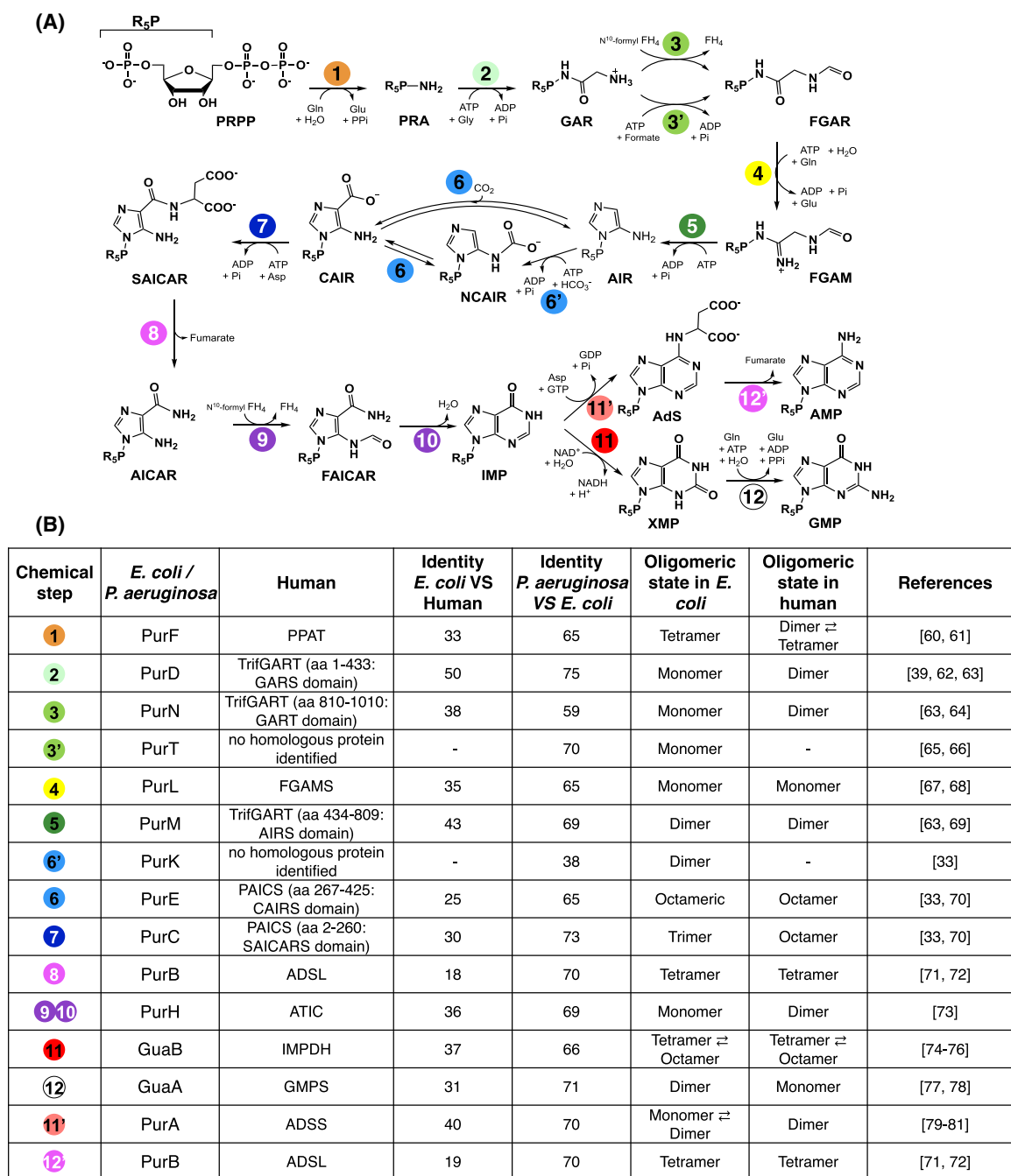


Fig. 1. *de novo* biosynthetic pathway of purine nucleotides. (A) Schematic representation of the step-by-step conversion of PRPP to AMP and GMP. The chemical steps have been sequentially numbered and given a specific colour. (B) The enzymes implicated in each step are listed for two bacteria (*E. coli* and *P. aeruginosa*) and for mammals (human). In mammals, six enzymes are involved in the conversion of PRPP to IMP: PRPP amidotransferase (PPAT), TrifGART [trifunctional: GAR synthetase domain (GARS), GAR formyltransferase domain (GAR Tfase), AIR synthetase domain (AIRS)], FGAM synthase (FGAMS), PAICS [bifunctional: AICAR formyltransferase domain (AICAR Tfase), CAIR synthetase domain (CAIRS)], adenylosuccinate (ADSL), ATIC [bifunctional: AICAR formyltransferase domain (AICAR Tfase), IMP cyclohydrolase domain (IMPC)]. IMP is then processed into GMP by two reactions catalysed by inosine 5'-monophosphate dehydrogenase (IMPDH) and GMP synthase (GMPS), or into AMP by two other reactions catalysed by adenylosuccinate synthase (ADSS) and ADSL into AMP. In prokaryotes, the chemical steps are catalysed by 14 enzymes, annotated as PurF, PurD, PurN, PurT, PurL, PurM, PurK, PurE, PurC, PurB, PurH, IMPDH, GuaA and PurA. The sequence identities between the *E. coli* and human enzymes, or between the *E. coli* and *P. aeruginosa* enzymes, are also given, as well as the oligomeric states of each enzyme when it has been reported in the literature.

Results

To reveal interactions between the enzymes selected in this study, we employed a genetic approach using the BACTH system [28]. This technique relies on the interaction-mediated reconstitution of a functional adenylate cyclase from two complementary fragments (noted T25 and T18) of this enzyme (Fig. 2A). In this

system, the proteins of interest are fused to the T25 and T18 moieties and co-expressed in an *E. coli cyaA* strain (herein BTH101, see Table 1). Interactions between hybrid proteins are monitored by measuring the activity of β -galactosidase that is positively controlled by cyclic AMP (cAMP). All *E. coli* open reading frames (ORFs) encoding the enzymes of the *de novo* purine nucleotide biosynthesis pathway were

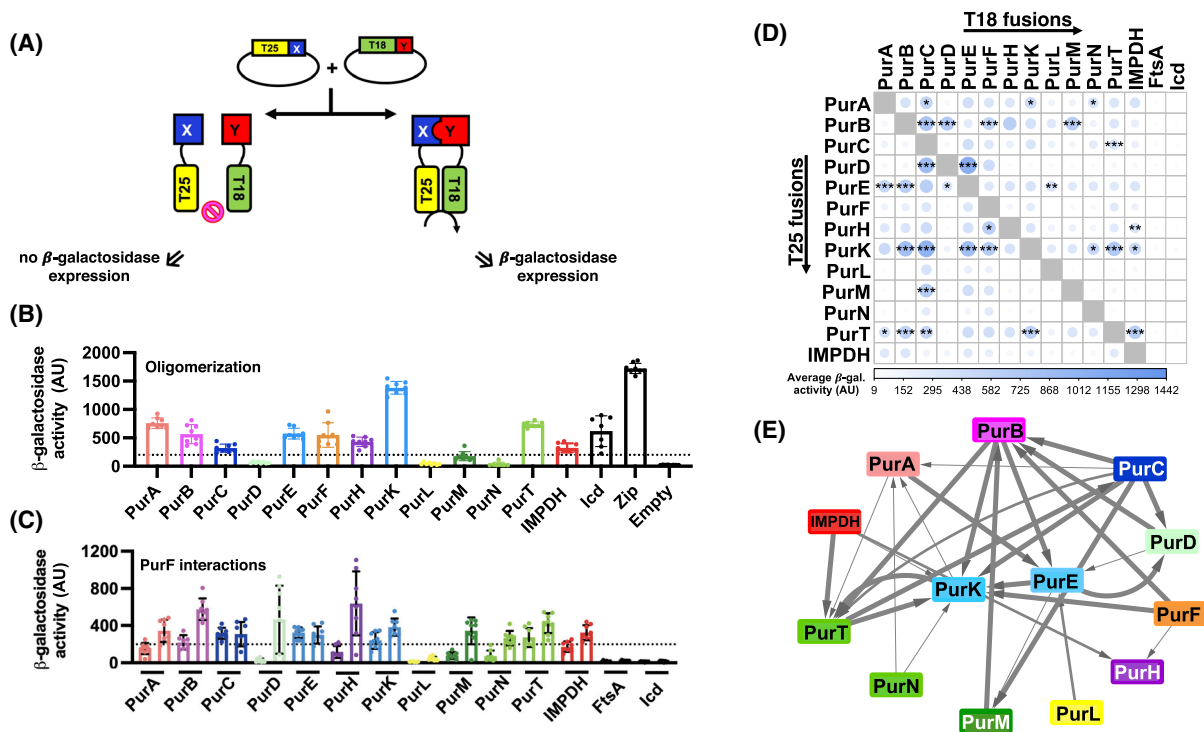


Fig. 2. Interaction network among the *E. coli de novo* purine nucleotide biosynthesis enzymes. (A) Principle of protein–protein interaction identification with the BACTH system. Each of the T25 and T18 fragments is fused with a protein of interest (noted X and Y) that are co-expressed in *E. coli cyaA* strain lacking adenylate cyclase. Interaction between proteins X and Y brings in close vicinity the complementary T25 and T18 fragments, reconstituting an adenylate cyclase activity. Thus, ATP is converted to cAMP, that activates the expression of the *lacZ* gene encoding β -galactosidase. β -galactosidase activity was measured on permeabilized bacteria as described in [Materials and methods](#). (B) BACTH analysis of the oligomerization state using co-expression of T25 and T18 fusions of the same enzyme (same colour code as in Fig. 1). β -galactosidase activity values measured as described in [Materials and methods](#) are presented in arbitrary units (A.U.). All mean and standard deviation data ($n = 8$) are available in Table 2. β -galactosidase activity values for the positive and negative controls (T25-Zip/T18-Zip and T25-Empty/T18-Empty combinations respectively) are 1723 AU \pm 90 and 23 AU \pm 4 respectively. The dotted line corresponds to fourfold the value of negative controls. (C) BACTH analysis (the same as in B) of interactions between PurF and all the other enzymes of the *de novo* purine nucleotide biosynthesis. Each enzyme (name given under the histogram, bars coloured with the same code as in Fig. 1) has been used as a prey either as a T25-fused (left) or T18-fused (right) protein and PurF as a bait (T18- or T25-fusion respectively). FtsA and Icd have been used in the same conditions as negative controls. (D) Two-dimensional adjusted *P*-value matrix representing significance of interactions measured by BACTH between the T25 (in column) and T18 (in line) versions of all the enzymes of interest. The intensity of the blue colour and the size of the circles are proportional to β -galactosidase activity values. An adaptive Benjamini–Hochberg procedure has been applied to get an adjusted *P*-value (a.*P*-value) in view to control the false discovery rate level. *, 1% < a.*P*-value < 5%; **, 0.1% < a.*P*-value < 1%; ***, a.*P*-value < 0.1%. (E) Interaction network where each arrow represents an interaction between enzymes identified by BACTH represented with Cytoscape 3.7 [50]. Each arrow represents a node between a T18 and a T25 version. The arrow's widths are proportional to the corresponding a.*P*-values. Protein oligomerizations (i.e. intra protein interactions) were not represented on the scheme. For mean, standard deviation values, and a.*P*-values, refer to Table 2. All data represent means \pm SD of the results from eight distinct measurements ($n = 8$).

Table 1. *E. coli* strains used in this study. BW25113, the parent strain from the Keio collection [30] has the following genotype: *lacI^f rrnB_{T14} ΔlacZ_{W116} hsdR514 ΔarraBAD_{AH33} ΔrhaBAD_{LD78}*.

Strain	Genotype	Source or reference
XL1-Blue	<i>F::Tn10 proAB⁺ lacI^f Δ(lacZ)M15 endA1 glnV44(AS) gyrA96 hsdR17 recA1 thi-1 lac</i>	Agilent technologies-stratagene
DH5α	<i>F⁻ (argF-lac)U169 o80Δ (lacZ)M15 deoR endA1 glnV44(AS) gyrA96 hsdR17 recA1 relA1 thi-1</i>	Laboratory collection
DHT1	<i>F- glnV44(AS) recA1 endA1 gyrA96 (naf) thi-1 hsdR17 spoT1 rfbD1 cya-854ilv-691::Tn10</i>	[56]
BTH101	<i>F⁻, cya-99, araD139, galE15, galK16, rpsL1, hsdR2, mcrA1, mcrB1</i>	[57]
BTH101Δ <i>purK</i>	BTH101 Δ <i>purK::kan</i>	This work
JW4135	BW25113 Δ <i>purA::kan</i>	[30]
JW2461	BW25113 Δ <i>purC::kan</i>	[30]
JW3969	BW25113 Δ <i>purD::kan</i>	[30]
JW0512	BW25113 Δ <i>purE::kan</i>	[30]
JW2309	BW25113 Δ <i>purF::kan</i>	[30]
JW3970	BW25113 Δ <i>purH::kan</i>	[30]
JW0511	BW25113 Δ <i>purK::kan</i>	[30]
JW2541	BW25113 Δ <i>purL::kan</i>	[30]
JW2484	BW25113 Δ <i>purM::kan</i>	[30]
JW2485	BW25113 Δ <i>purN::kan</i>	[30]
JW1838	BW25113 Δ <i>purT::kan</i>	[30]
JW2491	BW25113 Δ <i>guaA::kan</i>	[30]
JW5401	BW25113 Δ <i>guaB::kan</i>	[30]
<i>Ec-purKec</i>	JW0511Δ <i>purK kan::purKec</i> (of <i>E. coli</i>)	This work
<i>Ec-purKpa</i>	JW0511Δ <i>purK kan::purKpa</i> (of <i>P. aeruginosa</i>)	This work

cloned in-frame with the T25 or T18 fragment using a Gateway[®]-adapted BACTH system [29]. The expression and functionality of the fusion proteins were tested by complementation of *E. coli* mutant cells, deleted of the genes of interest (Keio collection [30] strains listed in Table 1), and therefore unable to grow on synthetic minimal medium (except the *purN* and *purT* mutants, as these enzymes are redundant). In all cases but GuaA (which was therefore excluded from the study), the expression of the T25- or T18-fused proteins could restore the growth of the *E. coli* mutants on minimal M63B1 medium indicating that their enzymatic activities were intact (Fig. 3).

For BACTH interaction assays, the T25 and T18 hybrids of each protein were co-expressed in BTH101 cells and their associations were monitored by measuring β-galactosidase activity in liquid cultures. As negative controls, in addition to the empty T25 and T18 fragments alone (noted empty in Fig. 2B), we used two cytosolic proteins unrelated to purine nucleotide metabolism: FtsA, a cell division protein, and isocitrate dehydrogenase (Icd), an enzyme involved in the TCA cycle. We also used the standard positive control of the BACTH system, T25-Zip and T18-Zip fusion proteins (Fig. 2B), with Zip being the leucine zipper of GCN4. Interaction signals were considered positive when β-galactosidase activity was at least four times higher than the signal measured with non-interacting control proteins.

Homo-oligomerization of each enzyme has been first tested: as shown in Fig. 2B, all the tested enzymes except PurD, PurL and PurN were able to dimerize including the control protein Icd known to be a homodimeric protein [31,32]. These observations were concordant with previously published data in *E. coli* showing the ability to oligomerize for each enzyme according to biochemical and biophysical characterizations (summarized in Fig. 1B). Then, we conducted a pairwise analysis of all possible interactions between the T25 and T18 hybrids. An example of BACTH assays conducted with PurF, the first enzyme of the pathway, is presented in Fig. 2C. The overall results of the tested interactions (see Table 2 for all the data) were further analysed by a two-dimensional statistical test, which results are shown as a two-dimensional matrix (Fig. 2D) and a network map (Fig. 2E). Noteworthy, T18-FtsA and T18-Icd have been used as negative prey controls and the measured β-galactosidase activity values were in the same range as those obtained with T25 and T18 fragments alone. We found that most of the enzymes are connected by multiple interactions, strongly suggesting that they could assemble *in vivo* into a multimolecular complex. Most interestingly, the bacterial-specific PurK enzyme appeared to interact with many of the *de novo* purine nucleotide biosynthesis enzymes, thus acting as a potential hub in this network, as well as PurE and

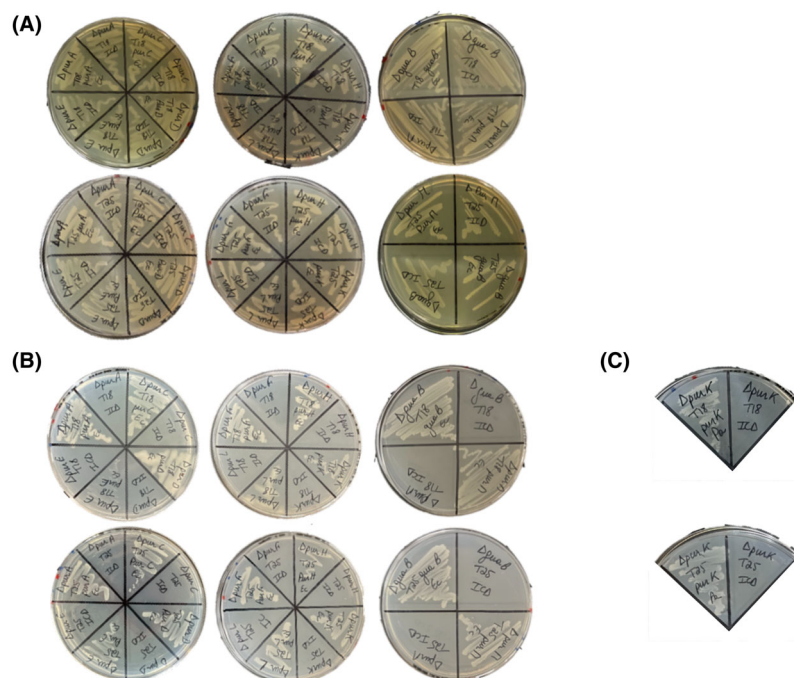


Fig. 3. Functional analysis of T25- and T18-fused proteins. Mutant strains deleted of the genes coding for the *de novo* purine nucleotide biosynthesis enzymes were obtained from the Keio collection [30]. Each mutant (Table 1) was transformed by either the pST25 or the pUT18C plasmid derivatives containing the corresponding deleted gene (Table 7) and the resulting transformants were plated on LB agar plates (as a growth control, panel A) or on M63B1 agar plates (panel B). Each deletion mutant was also transformed by pST25-*icd* or pUT18C-*icd* as negative controls to demonstrate the complementation selectivity. Thanks to the salvage pathway, the mutants are able to grow on LB medium (see panel A, growth in each sector) except for the $\Delta purB$ mutant that is also not able to grow on rich media (and was therefore not available). Yet, these mutants are unable to grow on minimum media (see panel B, no growth for each negative control strain transformed with *icd* gene) apart the $\Delta purN$ and $\Delta purT$ strains (not shown) as these two genes are redundant in *E. coli*. (C) The JW0511 strain was transformed with either the pST25 or the pUT18C plasmid derivatives containing the *P. aeruginosa purK* and plated on M63B1 agar plates. Same negative controls as in B.

PurC, the next two enzymes in the pathway. In total, our data suggest that *E. coli de novo* purine nucleotide biosynthetic enzymes can assemble into a multimolecular complex.

To explore whether the assembly of *de novo* purine nucleotide biosynthesis enzymes in a multicomplex could provide any physiological advantage to the cell, we attempted to specifically disrupt some key interactions by introducing appropriate mutations in one *pur* gene and characterize the biological consequences on the mutant. For that, we selected the *purK* gene, as its corresponding protein appears to interact with multiple enzymes of *de novo* purine nucleotide biosynthesis. In principle, one would use a PurK variant retaining full catalytic activity but impaired in its interaction with various *de novo* purine nucleotide biosynthesis enzymes. Instead of random mutagenesis, we have chosen the homologous PurK enzyme from *Pseudomonas aeruginosa* (noted PurKpa). Although PurKpa exhibits full enzymatic activity (as it is able to

complement the *E. coli purK* mutant in a minimal medium, Fig. 3C), it displays a low percentage of identity (Figs 1B and 4) with *E. coli* PurK (noted PurKec below), in particular at the protein surface (Fig. 4B), potentially involved in interaction with putative protein partners. To test our hypothesis, we performed the PurKpa interactome analysis and compared it with the PurKec one (Fig. 4C). For these BACTH assays, we constructed a BTH101 derivative strain (BTH101 $\Delta purK$), in which the endogenous *E. coli purK* gene was deleted in order to avoid competition between native PurKec and the T18-fused PurKec or the T18-fused PurKpa. As shown in Fig. 4C, PurKpa could not associate with PurC, PurF and PurM from *E. coli*, unlike PurKec. Thus, as hypothesized, PurKpa has an impaired interactome profile compared to that of PurKec.

To analyse the potential effect of disruption of the interaction network among the *de novo* purine nucleotide biosynthesis enzymes, we constructed an *E. coli*

Table 2. BACTH assays performed on eight colonies for each couple of T25 (row) and T18 (column) fusion proteins. (A) Means and standard deviations of the β -galactosidase activity measurements. (B) Adjusted P -values (a. P -values) calculated from the data listed in panel (A).

A	PurA	PurB	PurC	PurD	PurE	PurF	PurH	PurK	PurL	PurM	PurN	PurT	IMPDH	FtsA	Icd
PurA	759 ± 47	372 ± 73	559 ± 37	93 ± 17	430 ± 82	344 ± 60	327 ± 49	470 ± 86	150 ± 29	164 ± 40	372 ± 55	333 ± 56	373 ± 64	31 ± 4	4 ± 2
PurB	123 ± 45	769 ± 84	769 ± 82	695 ± 126	267 ± 76	576 ± 58	631 ± 206	399 ± 129	301 ± 69	660 ± 124	154 ± 41	326 ± 94	210 ± 71	36 ± 13	13 ± 9
PurC	158 ± 47	319 ± 23	319 ± 36	95 ± 41	428 ± 70	308 ± 65	201 ± 44	343 ± 44	179 ± 32	131 ± 17	251 ± 59	358 ± 18	194 ± 25	49 ± 24	10 ± 5
PurD	89 ± 11	892 ± 21	892 ± 81	67 ± 8	1070 ± 92	465 ± 183	55 ± 4	63 ± 8	59 ± 4	60 ± 8	56 ± 6	92 ± 29	82 ± 17	41 ± 4	15 ± 5
PurE	544 ± 61	626 ± 19	626 ± 98	362 ± 55	576 ± 47	299 ± 45	350 ± 58	370 ± 33	392 ± 44	275 ± 28	308 ± 74	283 ± 26	345 ± 33	19 ± 3	15 ± 3
PurF	154 ± 28	315 ± 35	315 ± 28	25 ± 9	323 ± 37	549 ± 101	118 ± 30	240 ± 42	12 ± 1	79 ± 17	74 ± 28	271 ± 47	173 ± 26	15 ± 4	12 ± 4
PurH	309 ± 23	454 ± 39	454 ± 53	46 ± 16	404 ± 73	637 ± 172	431 ± 42	325 ± 55	158 ± 41	178 ± 43	126 ± 26	274 ± 42	363 ± 32	35 ± 6	13 ± 4
PurK	487 ± 11	1016 ± 19	1017 ± 26	151 ± 8	862 ± 36	670 ± 86	382 ± 21	1381 ± 28	263 ± 21	319 ± 22	517 ± 13	730 ± 21	516 ± 16	54 ± 3	12 ± 3
PurL	37 ± 2	38 ± 3	381 ± 22	30 ± 2	207 ± 41	182 ± 20	24 ± 3	31 ± 6	45 ± 10	32 ± 4	21 ± 3	35 ± 5	87 ± 10	18 ± 3	9 ± 6
PurM	42 ± 8	682 ± 2	682 ± 67	45 ± 14	437 ± 86	344 ± 72	72 ± 16	89 ± 21	41 ± 6	178 ± 41	43 ± 12	109 ± 22	51 ± 22	21 ± 3	21 ± 9
PurN	53 ± 10	246 ± 8	246 ± 22	14 ± 4	136 ± 31	265 ± 38	32 ± 7	78 ± 14	11 ± 2	19 ± 5	37 ± 18	34 ± 9	25 ± 5	11 ± 2	5 ± 2
PurT	422 ± 52	565 ± 53	565 ± 20	53 ± 11	448 ± 65	425 ± 54	383 ± 52	604 ± 95	150 ± 24	344 ± 51	270 ± 39	737 ± 23	642 ± 64	34 ± 4	12 ± 3
IMPDH	30 ± 55	164 ± 72	164 ± 18	139 ± 41	270 ± 42	212 ± 43	115 ± 43	151 ± 30	68 ± 15	97 ± 39	94 ± 35	267 ± 32	325 ± 43	10 ± 3	17 ± 1
B	PurA	PurB	PurC	PurD	PurE	PurF	PurH	PurK	PurL	PurM	PurN	PurT	IMPDH	FtsA	Icd
PurA	0.785405	0.014152	0.014152	0.785405	0.767957	0.785405	0.530701	0.021635	0.785405	0.785405	0.020018	0.785405	0.171123	0.785405	0.785405
PurB	0.78541	4.13E-05	4.13E-05	4.02E-05	0.785405	0.000234	0.052502	0.785405	0.785405	0.000447	0.785405	0.785405	0.785405	0.785405	0.785405
PurC	0.78541	0.785405	0.785405	0.785405	0.226607	0.785405	0.785405	0.07657	0.785405	0.785405	0.507289	1.70E-05	0.785405	0.785405	0.785405
PurD	0.78541	0.785405	1.00E-07	1.00E-07	1.03E-10	0.239809	0.785405	0.785405	0.785405	0.785405	0.785405	0.785405	0.785405	0.785405	0.785405
PurE	9.00E-06	4.00E-14	0.052502	0.039901	0.785405	0.785405	0.595021	0.785405	0.004613	0.785405	0.785405	0.785405	0.785405	0.785405	0.785405
PurF	0.78541	0.785405	0.785405	0.785405	0.785405	0.785405	0.785405	0.785405	0.785405	0.785405	0.785405	0.706797	0.785405	0.785405	0.785405
PurH	0.23981	0.785405	0.785405	0.785405	0.77186	0.012331	0.785405	0.785405	0.785405	0.785405	0.785405	0.785405	0.003268	0.785405	0.785405
PurK	0.24458	0.000254	8.00E-13	0.785405	4.00E-14	0.000208	0.785405	0.785405	0.785405	0.785405	0.010601	4.10E-08	0.049075	0.785405	0.785405
PurL	0.78541	0.785405	0.785405	0.785405	0.785405	0.785405	0.785405	0.785405	0.785405	0.785405	0.785405	0.785405	0.785405	0.785405	0.785405
PurM	0.78541	0.785405	5.68E-05	0.785405	0.114735	0.485946	0.785405	0.785405	0.785405	0.785405	0.785405	0.785405	0.785405	0.785405	0.785405
PurN	0.78541	0.785405	0.785405	0.785405	0.785405	0.785405	0.785405	0.785405	0.785405	0.785405	0.785405	0.785405	0.785405	0.785405	0.785405
PurT	0.03266	2.21E-06	0.003266	0.785405	0.785405	0.785405	0.239809	0.000481	0.785405	0.265396	0.785405	0.785405	1.73E-07	0.785405	0.785405
IMPDH	0.06681	0.462482	0.785405	0.785405	0.785405	0.785405	0.785405	0.785405	0.785405	0.785405	0.785405	0.459804	0.785405	0.785405	0.785405

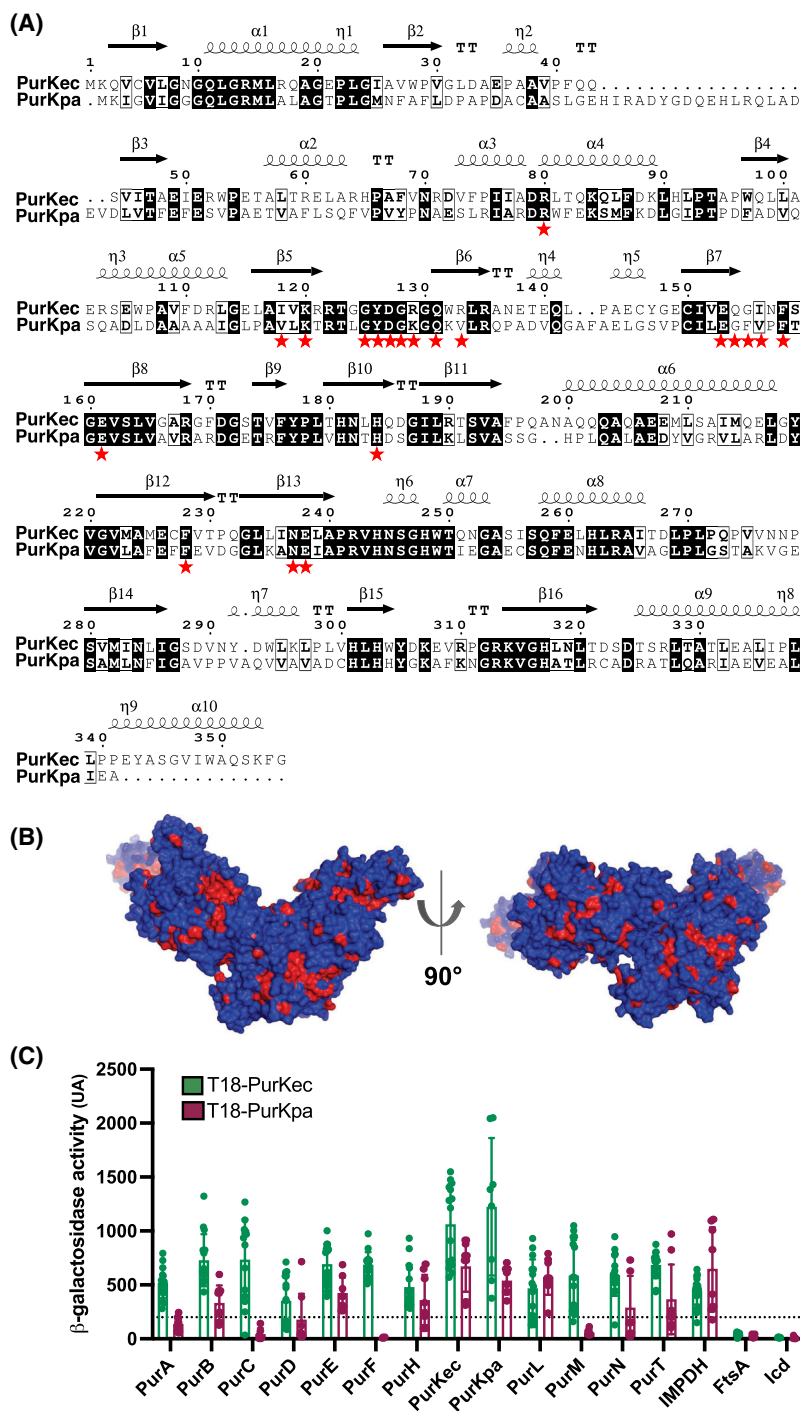


Fig. 4. Comparison of the *E. coli* PurK and *P. aeruginosa* PurK structures and interacting network profiles. (A) Sequence alignment of *E. coli* PurK (PurKec; UniProtKB entry P09029) and *P. aeruginosa* PurK (PurKpa; UniProtKB entry P72158). Secondary structure elements extracted from the PurKec crystal structure (PDB 1B6S) are indicated above the amino acid sequence and red stars indicate residues located within 4 Å of the ADP binding site. Alignment done with CLUSTAL W 2.0 [58] and ESPRIPT 3.0 [59]. (B) Amino acid conservations on 3D structure of PurKec (PDB 1B6S). Conserved residues are in red, and non-conserved residues are in blue. Representation done with PYMOL. (C) BACTH analysis of the interactions between T18-PurKec (in green) or T18-PurKpa (in purple) and the corresponding T25-versions of the *de novo* purine nucleotide biosynthesis enzymes. The fusions were co-expressed in BTH101 $\Delta purK$ strain. Data represent means \pm SD of the results from 16 distinct measurements ($n = 16$).

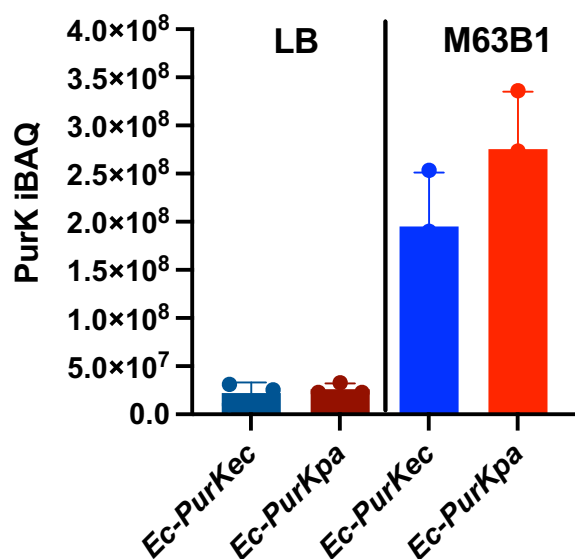


Fig. 5. Relative quantification by mass spectrometry of PurKec and PurKpa proteins from strains *Ec-PurKec* and *Ec-PurKpa*. Overnight culture of each strain was diluted into fresh LB or M63B1 medium. Aliquots at $OD_{600} = 0.3$ were used to perform the mass spectrometry experiments as described in the [Materials and methods](#) section. iBAQ values are defined as the sum of the intensities of all peptides detected after digestion by trypsin divided by the number of theoretical peptides for PurKec or PurKpa. Data represent means \pm SD of the results of three independent experiments ($n = 3$).

strain, *Ec-purKpa*, in which the native *purK* was replaced by the *P. aeruginosa purK* (by allelic exchange using the λ Red recombination system, see [Materials and methods](#)). As a control strain (noted *Ec-purKec* strain), the wild-type *E. coli purK* was similarly reintroduced in the same genetic background. First, by mass spectrometry, we checked the relative levels of PurKec or PurKpa proteins in the two strains *Ec-purKec* and *Ec-purKpa* under the same growth conditions. We found that these levels are equivalent between the two strains in the LB medium and in the minimal M63B1 medium, although the latter upregulates PurK expression as expected (Fig. 5). Then, we compared the specific activity of PurKec and PurKpa. For this purpose, both proteins were produced in *E. coli* as His-tagged proteins and purified as described in [Materials and methods](#) (Fig. 6A). Dynamic light scattering experiments were performed to optimize the buffer composition in order to increase the homogeneity of the protein samples: a common buffer was found suitable for both proteins. The catalytic activity was then measured using the coupled assay and reaction mixture described by Meyer *et al.* [33], using an 5-aminoimidazole ribonucleotide (AIR) substrate synthesized according to the synthesis scheme depicted in Fig. 6B. At fixed concentrations of both substrates (0.5 mM AIR and 1 mM ATP), PurKec and PurKpa

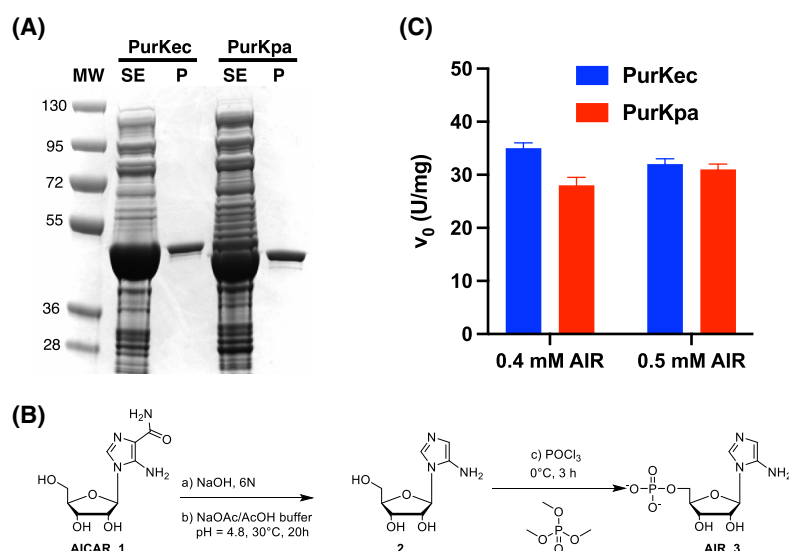


Fig. 6. Characterization of PurKec and PurKpa. (A) Recombinant His-tagged PurKec and PurKpa. Soluble extracts (SE) and 1 μ g of the purified fractions (P) after passage on a cobalt affinity resin and dialysis were loaded onto a 4–12% polyacrylamide-SDS gel and the proteins were visualized by Coomassie blue staining. (B) AIR synthesis scheme. Reaction conditions: (a) commercially available AICAR, NaOH 6 N (6 equiv.), refluxing for 4 h; (b) NaOAc/AcOH buffer, pH = 4.8, 30 °C, 20 h; (c) POCl₃ (10 equiv.), (MeO)₃PO, 0 °C, 3 h; 2. H₂O, NaOH. (C) Specific activity of PurKec and PurKpa at 1 mM ATP and two different concentrations of AIR (0.4 or 0.5 mM). The catalytic activity was measured at 37 °C using a coupled spectrophotometric assay as described in Meyer *et al.* [33]. Data represent means \pm SD of the results from three distinct measurements ($n = 3$).

exhibited similar specific activities (Fig. 6C; 32.5 ± 1.0 and $31 \pm 1 \text{ U} \cdot \text{mg}^{-1}$ respectively). Finally, we analysed the growth profile of the two strains *Ec-purKec* and *Ec-purKpa* in minimal medium, that is, in conditions where the *de novo* purine nucleotide biosynthesis is mandatory for bacterial growth. Two minimal media were used: the standard M63B1 and a derivative (noted M63B1*) with a lower concentration of MgCl_2 (see Materials and methods for exact composition). Magnesium (Mg^{2+}) is the most common divalent cation involved in the chelation of many cellular

components, in particular nucleotides and ATP, and in bacteria Mg^{2+} limitation impacts on ATP levels [34]. As shown in Fig. 7A (left part), the growth curves of both strains in M63B1 showed little difference when inoculated from stationary phase precultures (i.e. overnight cultures). Nucleotide quantifications, as well as adenylate and guanylate energy charges (Fig. 7B,C respectively), were also similar for both strains in this growth condition. On the other hand, when the cultures were inoculated from early log phase precultures, distinct growth curves were observed between the two

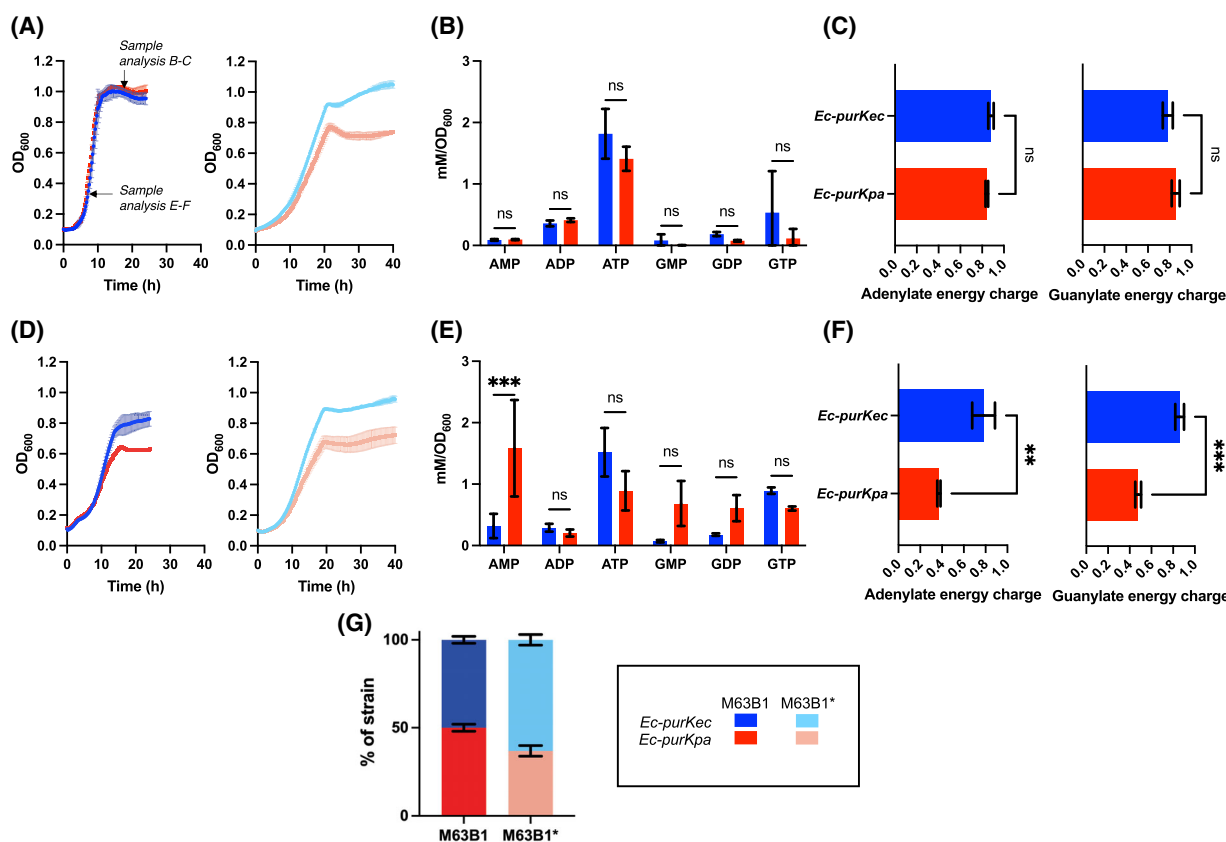


Fig. 7. The recombinant strains *Ec-purKec* and *Ec-purKpa* show differential bacterial fitness. (A) Representative growth curves of *Ec-purKec* (dark/light blue) and *Ec-purKpa* (red/pink) strains grown in M63B1 (left panel) or M63B1* (right panel). Each culture was inoculated from stationary phase precultures (i.e. overnight cultures) into 1 mL of M63B1 or M63B1* medium at an initial OD₆₀₀ of 0.1. Optical density measurement was done every 15 min. Aliquots at two time points (as indicated in the left panel) have been taken to quantify the intracellular concentrations of adenylate and guanylate nucleotides and used to calculate the adenylate and guanylate energetic charges. (B) Quantification of intracellular adenylate and guanylate nucleotides for the cultures of *Ec-purKec* (dark blue) and *Ec-purKpa* (red) strains in stationary phase grown in M63B1 medium. Reported values correspond to calculated concentrations normalized to the OD₆₀₀ of each bacterial sample. Changes were noted as significant according to a two-way ANOVA test: 0.12 (ns), 0.033 (*), 0.002 (**), < 0.001 (***). (C) Energetic charges of adenylate and guanylate calculated from nucleotide pool quantifications from B (the same colour code for the strains). Energy charges values were calculated as follows: $(\text{NTP} + 0.5 \text{ NDP}) / (\text{NTP} + \text{NDP} + \text{NMP})$ with N = A or G. Changes were noted as significant according to a Mann–Whitney test: 0.12 (ns), 0.033 (*), 0.002 (**), < 0.001 (***). (D) Same as in A, but with cultures inoculated from early log phase precultures. (E) same as in B, but with culture in early log phase, as indicated in panel A. (F) Same as in C, but with data from E. (G) Competition assay of *Ec-purKec* and *Ec-purKpa* strains grown in M63B1 or M63B1*. Overnight precultures in stationary phase were used to inoculate the co-culture (1 : 1 ratio). All reported data of this figure represent means \pm SD of the results from three independent experiments ($n = 3$).

strains (Fig. 7D, left part). The growth rate of the *Ec-purKpa* strain slows down few hours earlier than that of the *Ec-purKec* strain, and the final OD₆₀₀ of the former strain is lower than that of the latter. Additionally, when samples were taken from early log phase culture (see Fig. 7A), nucleotide quantifications (Fig. 7E) revealed modifications in adenylate and guanylate energy charges (Fig. 7F): 2.1- and 1.8-fold decrease, respectively, in *Ec-purKpa* as compared to *Ec-purKec*. Interestingly, the growth curves in M63B1*, the minimal medium with Mg²⁺ limitation, show the same trend regardless of the growth phase (stationary or exponential; see the curves on the right in Fig. 7A,D respectively) used for the inoculum. Moreover, when grown in co-culture with the *Ec-purKpa* strain in M63B1* medium, the *Ec-purKec* strain showed a clear growth advantage (Fig. 7G). Taken together, these results indicate that the disruption of few interactions between PurK and the *de novo* purine nucleotide biosynthesis enzymes had a significant effect on the bacterial growth and fitness and influenced the purine nucleotide pools. As the decrease in nucleotide energetic charges is directly linked to a reduction in anabolic metabolism according to the Atkinson principle [35,36], our results thus indicate that alterations of the interaction network in the assembly of *de novo* purine nucleotide biosynthesis enzymes result in dysregulation in purine nucleotide metabolism.

Discussion

Cellular compartmentalization has long been considered an exclusive eukaryotic feature. However, the description of several compartments in bacteria has resulted in the generalization of this notion to all living organisms [37]. Other compartments, already described in eukaryotes, have more recently been found in bacteria such as phase separations [38] or metabolons [6].

Here, using a two-hybrid approach, we demonstrate a dense protein interaction network among all the enzymes of the *E. coli de novo* purine nucleotide biosynthesis, including enzymes from the committed step and the branching towards AMP and GMP synthesis. Prior studies have suggested potential interactions between certain *de novo* purine nucleotide biosynthesis enzymes, although direct biochemical evidence for such associations has never been provided. Rudolph and Stubbe [27] proposed from a detailed kinetic analysis that the *E. coli* PurF and PurD enzymes may transiently interact to facilitate direct transfer (i.e. channelling) of the PRA intermediate (see Fig. 1) from one

enzyme to the other. Subsequently, a docking model of the two enzymes was proposed to account for the observed channelling specificity [39]. However, the same authors [27] were unable to demonstrate a stable protein–protein association. In our study, we could detect an interaction between PurF and PurD (in one configuration, see Fig. 2D and Table 2) and, in addition, we found that both proteins associate with several *de novo* purine nucleotide biosynthesis enzymes. These latter thus might stabilize the PurF/PurD association to facilitate PRA channelling. It was also speculated that in *E. coli* PurL might be a scaffold for the formation of a complex based on structural data of two PurL variants: a large version found in gram-negative bacteria [40] and a small PurL (noted smPurL) in gram-positive bacteria which form a complex with two other proteins, PurQ and PurS [41]. A complex could be reconstituted from the three isolated components from *B. subtilis* (yielding a large version of PurL, homologous to the gram-negative bacteria counterparts), while no complex could ever be obtained with the *E. coli* PurL and/or any other *de novo* purine nucleotide biosynthesis enzymes. On a larger scale, interatomic studies using affinity-purification of tagged protein in *E. coli* also failed to detect stable associations between *de novo* purine nucleotide biosynthesis enzymes [42]. This suggests that the interactions detected here by the BACTH system may be transient or of low affinity, and likely not stable enough to be detected by classical biochemical assays once the bacterial cells have been broken [43]. As the two-hybrid technique works in native bacteria where the hybrid proteins are confined inside cells, it may be more favourable to reveal associations of low affinity and/or of more dynamical character.

Our results further reveal significant differences in the topology of the *E. coli de novo* purine nucleotide biosynthesis assembly as compared to the early report on the human one, established by a Tango PPI two-hybrid assay [44]. First, no interactions between the three *E. coli* monofunctional enzymes PurD, PurN and PurM have been found, while their human homologues are fused in the trifunctional enzyme TrifGART. Furthermore, the core of the bacterial complex seems to be organized by PurE, PurK and PurC catalysing steps 6, 6' and 7, respectively, instead of PPAT, TrifGART and FGAMS in humans catalysing steps 1–5. Intriguingly, a recent report [45] from the same group showed that PAICS (catalysing steps 6 and 7 catalysed by PurE and PurC in *E. coli* respectively; see Fig. 1) interacts with eight of the nine enzymes of the *de novo* purine nucleotide pathway,

and therefore seems to have a central position in the metabolon. These new findings suggest that the molecular architecture of the human purinosome might share more similarities with the purine biosynthetic enzyme assembly found here in *E. coli*, although in the latter the specific bacterial component PurK, which does not have a human homologue, plays a central role.

In human cells, previous studies have shown the importance of protein–protein interactions in nucleotide biosynthesis. Several point mutations linked to neuropathology have been described in several alleles encoding ATIC, ADSL or PAICS [46–48]. In some cases, enzymatic activities were not altered, but the purinosome formation was impaired, illustrating the physiological importance of this complex in eukaryotic cells. Here, we also show that the proper assembly of the *E. coli* complex is crucial for maintaining the purine nucleotide pools and bacterial fitness. For this, we characterized an *E. coli* mutant strain in which the native PurKec was replaced by the *P. aeruginosa* counterpart PurKpa that displays loss of interactions with several *E. coli de novo* purine nucleotide biosynthesis partners. The growth curves of the two strains *Ec-purKec* and *Ec-purKpa* exhibit different profiles when starting from early log phase precultures in the two minimal media used in our study. Nucleotide quantification also revealed a change in the energy load of adenyl and guanylyl nucleotides during the exponential phase, due to cytoplasmic accumulation of AMP and GMP.

In total, our data support the idea that proper associations between the *de novo* purine nucleotide biosynthesis enzymes may provide a significant growth advantage for *E. coli* when this pathway is essential for survival. Further experiments will be necessary to better define the metabolic conditions where clustering of these enzymes is essential, and to explore how the interactions of *de novo* purine nucleotide biosynthesis proteins might facilitate the channelling of intermediates between the enzymes. Interfering with the assembly of this complex by using small molecule inhibitors of specific protein–protein interactions might open new perspectives for the development of novel antibiotics.

Materials and methods

Materials and general methods

Chemicals were purchased from Sigma-Aldrich (Saint-Louis, MO, USA). Phusion™ High-Fidelity DNA Polymerase and PCR reagents were purchased from Thermo Fisher Scientific (Waltham, MA, USA). Oligonucleotides (Tables 3–5) were ordered from Sigma-Aldrich. Restriction enzymes and Gateway recombination mixtures were purchased from Thermo Fisher Scientific and Invitrogen (Waltham, MA, USA) respectively. Genomic DNA from *E. coli* K12 MG1665 or *P. aeruginosa* PAO1 was used as PCR templates. PCR clean-up was performed with a QIAquick PCR Purification kit from Qiagen (Hilden, Germany). Plasmid purification was conducted with a GeneJET Plasmid Miniprep kit from Thermo Fisher Scientific. All recombinant plasmids were verified by restriction profiles and DNA sequencing (Eurofins Genomics, Les Ulis, France). For microbiology experiments, lysogeny broth (LB – 10 g·L⁻¹ peptone, 5 g·L⁻¹ yeast extract, 10 g·L⁻¹ NaCl, pH 7), minimal medium (M63B1–13.6 g·L⁻¹ potassium hydrogen phosphate, 0.2% ammonium sulfate, 0.01% magnesium sulfate, 0.025% iron sulfate, 0.002% thiamine hydrochloride, 0.2% glucose, pH 7) or minimal medium with low concentration of magnesium (M63B1*, same composition as M63B1 but with 0.025 mM of magnesium instead of 0.4 mM) were used. For plates, 15 g·L⁻¹ of agar was added to the medium with the appropriate antibiotics. Bacterial growth was monitored by measurement of optical density at 600 nm with an automated UVmcl spectrophotometer (SAFAS, Monaco, Monaco).

Bacterial strains

Bacterial strains used in this study are listed in Table 1. The *E. coli* XL-1 Blue, DH5α and DHT1 strains were used for routine cloning experiments. BACTH complementation assays were carried out with the *E. coli cyaA* strains BTH101, or the derivative BTH101Δ*purK*. Strain BTH101Δ*purK* in which the *purK* ORF was replaced by kanamycin resistance markers (Δ*purK::kan*) was constructed by P1 transduction technique using JW0511 strain (refer to Table 1) from the Keio collection [30]. Transductants were selected on LB agar plates supplemented with kanamycin (50 μg·mL⁻¹). The *Ec-purKec* and *Ec-purKpa* strains were used for physiological studies. In these

Table 3. Oligonucleotides used for bacterial strains construction.

Strain	Sequence (5' – 3')
<i>Ec-purKec</i>	Forward GACTGGCGCAAAGCCAGACCGACGAAGTGC TGAAAAACCCGGACCCGGAGGTGCGGCATGAAACAGGTTTGCGTCCTCGG
	Reverse GGTACCGGATCGGTAGGCCGGATAAGGCGTTTACGCCGCATCCGGCAAGAATAGAGCACCAGTTAACCGAACCTACTCTGCGCCCAATCACGC
<i>Ec-purKpa</i>	Forward GACTGGCGCAAAGCCAGACCGACGAAGTGC TGAAAAACCCGGACCCGGAGGTGCGGCATGAAATCGGTGTCATCGGTGG
	Reverse GGTACCGGATCGGTAGGCCGGATAAGGCGTTTACGCCGCATCCGGCAAGAATAGAGCACCAGTTCACGCCTCGATCAGCCCTCGACC

Table 4. Oligonucleotides used for pDONR201 constructions.

Construct	Sequence (5' – 3')	
pDONR201- <i>purD</i>	Forward	GGGGACAAGTTTGTACAAAAAGCAGGCTTAATGAAAGTATTAGTGATTGGTAACGG
	Reverse	GGGGACCACCTTTGTACAAGAAAGCTGGGTTTTAGTTCTGCTCGCGTTCGATAGC
pDONR201- <i>purL</i>	Forward	GGGGACAAGTTTGTACAAAAAGCAGGCTTAATGATGAAATTCGCGTGGTTCCG
	Reverse	GGGGACCACCTTTGTACAAGAAAGCTGGGTTTTACCCCAACTGCTTACGCGCATTGC
pDONR201- <i>icd</i>	Forward	GCCGCACAAGTTTGTACAAAAAGCAGGCTTTATGGAAAGTAAAGTAGTTGTTCCGGCACAAG
	Reverse	GCGGACCACCTTTGTACAAGAAAGCTGGGTTTTACATGTTTCGATGATCGCGTCACC
pDONR201- <i>purKpa</i>	Forward	GGGGACAACCTTTGTACAAAAAGCAGGCTTAATGAAATCGGTGTCATCGGTGG
	Reverse	GGGGACCACCTTTGTACAAGAAAGCTGGGTTTCACGCTCGATCAGCGCC

Table 5. Oligonucleotides used for identification of *Ec-purKec* and *Ec-purKpa* strains for competition assays.

Primer	Sequence (5' – 3')
Forward <i>purK</i>	GAAAACCCGGACCCGCGAGG
Reverse <i>purKec</i>	GCTCGCGGGTTAATGCGG
Reverse <i>purKpa</i>	GCCGGCTGGCGCAGGACC

strains, the kanamycin resistance marker of JW0511 was replaced with *purK* gene of *P. aeruginosa* (*purKpa*) or *purK* gene of *E. coli* (*purKec*) by using the Red recombination system (Gene Bridges, Heidelberg, Germany). For this, *purK* ORFs were PCR-amplified from the corresponding genomic DNAs, adding terminal homology stretches of 50 bp (Table 3 for sequences). The purified PCR products were then introduced by electroporation into electro-competent JW0511 cells carrying the plasmid pRedET (Gene Bridges). Recombinant clones were selected on M63B1 agar plates and after re-isolation, correct insertions were verified by sequencing.

Plasmid construction

Plasmids used in this study are listed in Tables 6–8. The Gateway cloning method (Thermo Fisher Scientific; Invitrogen) was used for the construction of the BACTH recombinant plasmids. The *E. coli purD*, *purL* and *icd* genes, and the *P. aeruginosa purK* gene were amplified by PCR using specific oligonucleotides carrying *attB* sequences (Table 4) and cloned into pDONR201 (Thermo Fisher Scientific; Invitrogen) with the BP clonease II mix as recommended by the manufacturer (Gateway® BP Clonease™ Enzyme mix, Invitrogen). All other ORFs were purchased from Twist Bioscience (San Francisco, CA, USA) as synthetic genes (flanked by the appropriate *attB* sequences) inserted into the Gateway entry vector pTwist-ENTR (Table 6). Cloning of each gene from the *attL*-flanked pDONR201 or pTwist-ENTR vectors into the *attR*-flanked destination vectors pST25-DEST or pUT18C-DEST [29] was done with the LR clonease II mix (Gateway® LR Clonease™ Enzyme mix, Invitrogen), in which the ORFs were

Table 6. Donor vectors used in this study.

Plasmid	Description	Source
pDONR201	Gateway entry vector for inserting an <i>attB</i> -flanked gene	Thermofisher Scientific (Laboratory collection)
pTwist-ENTR	Gateway entry vector	Twist bioscience
pTwist- <i>purA</i>	pTwist-ENTR harbouring the ORF of <i>purA</i> of <i>E. coli</i>	This work
pTwist- <i>purB</i>	pTwist-ENTR harbouring the ORF of <i>purB</i> of <i>E. coli</i>	This work
pTwist- <i>purC</i>	pTwist-ENTR harbouring the ORF of <i>purC</i> of <i>E. coli</i>	This work
pDONR201- <i>purD</i>	pDONR201 harbouring the ORF of <i>purD</i> of <i>E. coli</i>	This work
pTwist- <i>purE</i>	pTwist-ENTR harbouring the ORF of <i>purE</i> of <i>E. coli</i>	This work
pTwist- <i>purF</i>	pTwist-ENTR harbouring the ORF of <i>purF</i> of <i>E. coli</i>	This work
pTwist- <i>purH</i>	pTwist-ENTR harbouring the ORF of <i>purH</i> of <i>E. coli</i>	This work
pTwist- <i>purKec</i>	pTwist-ENTR harbouring the ORF of <i>purK</i> of <i>E. coli</i>	This work
pDONR201- <i>purKpa</i>	pDONR201 harbouring the ORF of <i>purK</i> of <i>P. aeruginosa</i>	This work
pDONR201- <i>purL</i>	pDONR201 harbouring the ORF of <i>purL</i> of <i>E. coli</i>	This work
pTwist- <i>purM</i>	pTwist-ENTR harbouring the ORF of <i>purM</i> of <i>E. coli</i>	This work
pTwist- <i>purN</i>	pTwist-ENTR harbouring the ORF of <i>purN</i> of <i>E. coli</i>	This work
pTwist- <i>purT</i>	pTwist-ENTR harbouring the ORF of <i>purT</i> of <i>E. coli</i>	This work
pTwist- <i>guaA</i>	pTwist-ENTR harbouring the ORF of <i>guaA</i> of <i>E. coli</i>	This work
pTwist- <i>guaB</i>	pTwist-ENTR harbouring the ORF of <i>guaB</i> of <i>E. coli</i>	This work
pDONR201- <i>icd</i>	pDONR201 harbouring the ORF of <i>icd</i> of <i>E. coli</i>	This work

Table 7. BACTH vectors used in this study.

Plasmid	Description	Source or reference
pST25-DEST	BACTH destination vector for cloning ORF of interest at the C-terminus of T25; p15 <i>ori</i> , Spc ^r	[29]
pUT18C-DEST	BACTH destination vector for cloning ORF of interest at the C-terminus of T18; ColE1 <i>ori</i> , Amp ^r	[29]
pST25- <i>purA</i>	pST25-DEST harbouring <i>purA</i> of <i>E. coli</i>	This work
pST25- <i>purB</i>	pST25-DEST harbouring <i>purB</i> of <i>E. coli</i>	This work
pST25- <i>purC</i>	pST25-DEST harbouring <i>purC</i> of <i>E. coli</i>	This work
pST25- <i>purD</i>	pST25-DEST harbouring <i>purD</i> of <i>E. coli</i>	This work
pST25- <i>purE</i>	pST25-DEST harbouring <i>purE</i> of <i>E. coli</i>	This work
pST25- <i>purF</i>	pST25-DEST harbouring <i>purF</i> of <i>E. coli</i>	This work
pST25- <i>purH</i>	pST25-DEST harbouring <i>purH</i> of <i>E. coli</i>	This work
pST25- <i>purKec</i>	pST25-DEST harbouring <i>purK</i> of <i>E. coli</i>	This work
pST25- <i>purKpa</i>	pST25-DEST harbouring <i>purK</i> of <i>P. aeruginosa</i>	This work
pST25- <i>purL</i>	pST25-DEST harbouring <i>purL</i> of <i>E. coli</i>	This work
pST25- <i>purM</i>	pST25-DEST harbouring <i>purM</i> of <i>E. coli</i>	This work
pST25- <i>purN</i>	pST25-DEST harbouring <i>purN</i> of <i>E. coli</i>	This work
pST25- <i>purT</i>	pST25-DEST harbouring <i>purT</i> of <i>E. coli</i>	This work
pST25- <i>guaA</i>	pST25-DEST harbouring <i>guaA</i> of <i>E. coli</i>	This work
pST25- <i>guaB</i>	pST25-DEST harbouring <i>guaB</i> of <i>E. coli</i>	This work
pKT25- <i>ftsA</i>	pKT25 harbouring <i>ftsA</i> of <i>E. coli</i>	[57]
pST25- <i>icd</i>	pST25-DEST harbouring <i>icd</i> of <i>E. coli</i>	This work
pKT25- <i>zip</i>	pKT25 encoding Zip, the leucine zipper region of the yeast protein GCN4	[28]
pUT18C- <i>purA</i>	pUT18C-DEST harbouring <i>purA</i> of <i>E. coli</i>	This work
pUT18C- <i>purB</i>	pUT18C-DEST harbouring <i>purB</i> of <i>E. coli</i>	This work
pUT18C- <i>purC</i>	pUT18C-DEST harbouring <i>purC</i> of <i>E. coli</i>	This work
pUT18C- <i>purD</i>	pUT18C-DEST harbouring <i>purD</i> of <i>E. coli</i>	This work
pUT18C- <i>purE</i>	pUT18C-DEST harbouring <i>purE</i> of <i>E. coli</i>	This work
pUT18C- <i>purF</i>	pUT18C-DEST harbouring <i>purF</i> of <i>E. coli</i>	This work
pUT18C- <i>purH</i>	pUT18C-DEST harbouring <i>purH</i> of <i>E. coli</i>	This work
pUT18C- <i>purKec</i>	pUT18C-DEST harbouring <i>purK</i> of <i>E. coli</i>	This work
pUT18C- <i>purKpa</i>	pUT18C-DEST harbouring <i>purK</i> of <i>P. aeruginosa</i>	This work
pUT18C- <i>purL</i>	pUT18C-DEST harbouring <i>purL</i> of <i>E. coli</i>	This work
pUT18C- <i>purM</i>	pUT18C-DEST harbouring <i>purM</i> of <i>E. coli</i>	This work
pUT18C- <i>purN</i>	pUT18C-DEST harbouring <i>purN</i> of <i>E. coli</i>	This work
pUT18C- <i>purT</i>	pUT18C-DEST harbouring <i>purT</i> of <i>E. coli</i>	This work
pUT18C- <i>guaA</i>	pUT18C-DEST harbouring <i>guaA</i> of <i>E. coli</i>	This work
pUT18C- <i>guaB</i>	pUT18C-DEST harbouring <i>guaB</i> of <i>E. coli</i>	This work
pUT18C- <i>ftsA</i>	pUT18C harbouring <i>ftsA</i> of <i>E. coli</i>	[57]
pUT18C- <i>icd</i>	pUT18C-DEST harbouring <i>icd</i> of <i>E. coli</i>	This work
pUT18C- <i>zip</i>	pUT18C encoding Zip, the leucine zipper region of the yeast protein GCN4	[28]

recombined in-frame with the T25 or T18 fragments of the adenylate cyclase of *Bordetella pertussis* (Table 7).

Similarly, for PurKec and PurKpa overproduction in *E. coli*, the expression vectors p17-*purKec* and p17-*purKpa* (Table 8) were constructed by recombining ORFs, respectively, from the pTwist-*purKec* or pDONR201-*purKpa* donor vectors into the destination vector pDEST17 (Thermo Fisher Scientific).

BACTH assay

Identification of protein–protein interactions was conducted with the BACTH complementation assay, where each biosynthetic enzyme was fused with the T25 or T18 fragments

of the catalytic domain of *B. pertussis* adenylate cyclase and co-expressed in the BTH101 strain. Chemically competent bacteria were co-transformed with one pST25-DEST derivative and one pUT18C-DEST derivative and plated on LB agar supplemented with appropriate antibiotics, 0.5 mM IPTG and 40 $\mu\text{g}\cdot\text{mL}^{-1}$ of X-gal and incubated at 30 °C for 36 to 72 h.

For each pair of hybrid proteins, eight individual clones were selected and adenylate cyclase reconstitution was followed as previously described [49] by β -galactosidase activity quantifications for 6 min following ortho-nitrophenol formation. Measurements were performed on a Sunrise plate reader (TECAN, Männedorf, Switzerland) equipped with two filters (405 and 595 nm).

Table 8. PurKec and PurKpa expression vectors used in this study.

Plasmid	Description	Source or reference
pDEST17	Destination vector for cloning ORF of interest with a 6His-tag at the N-terminus; pBR322 <i>ori</i> , Amp ^r	ThermoFisher Scientific (Laboratory collection)
p17- <i>purKec</i>	pDEST17 harbouring <i>purK</i> from <i>E. coli</i>	This work
p17- <i>purKpa</i>	pDEST17 harbouring <i>purK</i> from <i>P. aeruginosa</i>	This work

Data were analysed with GRAPHPAD PRISM 5.0 software (San Diego, CA, USA). The relative activity of β -galactosidase expressed in arbitrary units (AU) was calculated according to the following formula:

$$\frac{(\text{OD}_{405\text{nm}} - \text{OD}_{405\text{nm}} \text{ Blank})/6}{(\text{OD}_{595\text{nm}} - \text{OD}_{595\text{nm}} \text{ Blank})} \times 1000.$$

A one-tailed *t*-test was used to evaluate if one average is superior to the averages of activity of T18 fragments of other proteins with T25 fragments, and another one-tailed *t*-test was used to evaluate if the average is superior to the averages of T25 fragments of other proteins with T18 fragments. The *P*-values of both tests were then merged using the Stouffer's method to create a combined *P*-value indicating if the estimated average is significantly superior to both the averages of T18 fragments of other proteins with T25 fragments, and the averages of T25 fragments of other proteins with T18 fragments. Merged *P*-values were further analysed with a Benjamini–Hochberg procedure to control the false discovery rate, resulting in adjusted *P*-values. Source data for means, standard deviations values and adjusted *P*-values are available in Table 2.

CYTOSCAPE 3.7 [50] was used to represent the interaction network (Fig. 2E) between all the enzymes of the *de novo* purine nucleotide biosynthesis.

With PurKpa series (Fig. 4C), the BACTH assays were carried out in a BTH101 derivative (noted BTH101 Δ *purK*) carrying a deletion of the chromosomal *purK* gene to avoid potential competition with the endogenous wild-type PurKec. The functionality of PurKpa T25- and T18- fusions was checked by complementation of the *E. coli* Δ *purK* strain. For comparison purposes, the same strain was used for the PurKec series.

Bacterial competition assay

Competition assays were performed by bacterial co-cultures. Briefly, the *Ec-purKec* and *Ec-purKpa* strains were grown separately overnight in M63B1 or M63B1*. Bacteria grown from a stationary phase overnight culture were diluted into fresh medium to an OD₆₀₀ of 0.05, mixed in

equal volume and incubated until exponential phase (i.e. OD₆₀₀ of around 0.5). The cell suspensions were then spotted on LB-agar plates and incubated at 37 °C. Initial and final proportions of each strain in the mixture were determined by PCR analysis of 20 randomly selected colonies (5 colonies per quadrant) using RedTaq Ready Mix (Sigma), 10 pmol of each of the 4 primers (listed in Table 5) and analysis by 1% agarose gel electrophoresis. Three independent experiments were performed for each medium.

Mass spectrometry

Ec-purKec and *Ec-purKpa* samples, grown in 5 mL of fresh M63B1 medium supplemented with 0.2% glucose and incubated at 37 °C, were harvested by centrifugation during the exponential phase (OD₆₀₀ ~ 0.3). Bacterial pellets were resuspended in 100 μ L of 8 M urea, 50 mM Tris–HCl pH7.5. After sonication, soluble fractions were digested with Sequencing grade Modified Trypsin at 37 °C. After purification of peptides on Sep-Pak C₁₈-SPE cartridges (Waters, Sevenoaks, UK), analysis was conducted in a Q Exactive Plus mass-spectrometer (Thermo Fisher Scientific) coupled with and Easy nLC-1200 chromatography system (Thermo Fisher Scientific).

Nucleotide pool analysis

Overnight cultures of *Ec-purKec* and *Ec-purKpa* strains were diluted 1 : 40 into 250 mL M63B1 supplemented with 0.2% glucose and incubated at 37 °C. Bacteria were harvested at 4 °C by centrifugation of 100 mL of medium at two different time points, the exponential phase (OD₆₀₀ ~ 0.3) and the stationary phase (OD₆₀₀ ~ 1.1–1.2). Pellets were deproteinized with an equal volume of 6% perchloric acid, vortex-mixed for 20 s, ice-bathed for 10 min and vortex-mixed again for 20 s. Supernatants recovered by centrifugation were then diluted 1 : 1 in bi-distilled water, vortex-mixed for 60 s and neutralized by the addition of 2 M Na₂CO₃. Extract analysis was performed on a 250 \times 4.6 mm C18 Supelco 5- μ m column (Sigma) in-line with an HPLC system (Shimadzu HPLC system interfaced with LABSOLUTION software, Marne-la-Vallée, France). Elution was conducted with a flow-rate of 1 mL·min⁻¹ with the following program: A–B (60 : 40) at 0 min \rightarrow (40 : 60) at 30 min \rightarrow (40 : 60) at 60 min. Buffer A contained 10 mM tetrabutylammonium hydroxide, 10 mM KH₂PO₄ and 0.25% MeOH, pH 6.9. Buffer B consisted of 5.6 mM tetrabutylammonium hydroxide, 50 mM KH₂PO₄ and 30% MeOH, pH 7.0. Solution detection was done with the diode array detector. Products were spectrophotometrically monitored at OD₂₅₄. Quantification was performed by integration of the peak absorbance areas, employing a calibration curve established with various known nucleotides. Nucleotide concentrations were normalized according to the initial

OD₆₀₀ of each bacterial sample. Nucleotide energy charges were calculated according to the following formula [35,36]:

$$\frac{[\text{NTP}] + 0.5 [\text{NDP}]}{[\text{NTP}] + [\text{NDP}] + [\text{NMP}]}$$

Production and purification of PurKec and PurKpa

PurKec and PurKpa recombinant proteins were expressed, respectively, from the p17-*purKec* and p17-*purKpa* constructs (Table 8) as fusion proteins with a His-tag at the N-terminus (MSYYHHHHHLESTSLYKKAG) in *E. coli* BL21(DE3)/pDIA17 strain [51]. Bacteria transformed with each corresponding plasmid were initially grown at 37 °C in 1 L of 2YT medium supplemented with 35 µg·mL⁻¹ kanamycin and 30 µg·mL⁻¹ chloramphenicol. In the case of PurKec, protein production was induced by adding 0.6 mM IPTG at OD₆₀₀ ~ 0.5 and bacteria were transferred to a 16 °C shaker and left for growth overnight. In the case of PurKpa, protein production was induced by adding 1 mM of IPTG at OD₆₀₀ ~ 1.3 to the growing culture and leaving for growth for 4 h at 37 °C. Bacteria were harvested by centrifugation for 30 min at 15 000 *g*.

Bacterial pellet was resuspended in buffer A (50 mM Tris-HCl pH 8, 100 mM KCl) supplemented with a cOmplete™ ULTRA EDTA-free protease inhibitor tablet (Roche Diagnostics, Bâle, Switzerland) and lysed by sonication with a Bioblock Scientific Vibra Cell. After centrifugation at 10 000 *g* for 1 h, the soluble fraction was added to a TALON metal affinity resin (TaKaRa Bio USA, Inc., Saint-Germain-en-Laye, France). The next steps were conducted as recommended by the manufacturer using the batch/gravity—flow column purification procedure [52] at room temperature. Proteins were eluted with buffer A supplemented with 150 mM imidazole. All eluted fractions were pooled and further dialysed in buffer A supplemented with 1 mM DTT and 1 mM EDTA. Protein concentration was determined using the molar absorption coefficient (60 180 and 21 680 M⁻¹·cm⁻¹ for PurKec and PurKpa respectively) predicted from the amino acid sequence by the PROTPARAM tool [53]. Dynamic light scattering experiments were performed on a DynaPro plate reader (Wyatt Technology, Toulouse, France) to verify protein qualities in buffer A.

AIR synthesis and enzymatic assay for PurK enzymes

The 5-amino-1-β-ribofuranosylimidazole 5'-monophosphate (AIR, **3**; see scheme, Fig. 6B) was prepared from commercially available 5-aminoimidazole-4-carboxamide ribonucleotide (AICAR) as previously described. Briefly, AICAR was saponified in 6 N NaOH according to the method of Srivastava *et al.* [54] to afford sodium 5-amino-1-(β-ribofuranosyl)imidazole-4-carboxylate which was then converted to the

enamino acid and decarboxylated in a pH 4.8 aqueous NaOAc/AcOH buffer [55] to afford **2**. AIR (**3**) was then obtained after phosphorylation of **2** with POCl₃ as described in Meyer *et al.* [33]. Spectral data of compounds **2** and **3** were in accordance with previously published data.

AIR was resuspended in 50 mM HEPES pH 7.8, 20 mM KCl and the concentration was calculated using an extinction coefficient of 1570 M⁻¹ cm⁻¹ at 260 nm [33].

The catalytic activity of PurKec and PurKpa was measured using an enzyme-coupled spectrophotometric assay as previously described by Meyer *et al.* [33]. The reaction medium (total volume 0.5 mL) contained 50 mM HEPES pH 7.8, 20 mM KCl, 6 mM MgCl₂, 1 mM ATP, 2 mM phosphoenolpyruvate, 0.32 mg·mL⁻¹ NADH, 10 units of pyruvate kinase, 5 units of lactate dehydrogenase, and either 0.4 or 0.5 mM AIR. The reaction was started by the addition of the enzyme (1.6 µg, diluted in buffer A). Measurements were conducted at 37 °C on an Eppendorf ECOM 6122 photometer by monitoring the formation of NADH at 340 nm. One unit of enzyme activity is defined as 1 µmole of the product formed in 1 min.

Acknowledgements

We are grateful to Jean-Marc Ghigo for providing the *E. coli* mutant strains from the Keio collection. We thank Cécile Philippon for participation in BACTH assays. We thank the 'Plateforme de Milieu' of the Institut Pasteur for media culture preparations. We thank the Molecular Biophysics facility and the Proteomic platform of the Institut Pasteur, and in particular Sébastien Brûlé for the DLS experiments, and Mariette Matondo and Magalie Duchateau for the mass spectrometry experiments. Laurence Dugué is acknowledged for participation in the AIR synthesis and purification. We thank Françoise Norel for fruitful discussions. This work was supported in part by the Centre National de la Recherche Scientifique (CNRS), the Institut National de la Santé Et de la Recherche Médicale (INSERM), and the Institut Pasteur. Antoine Gedeon and Nour Ayoub acknowledge PhD fellowships from the Médicament, Toxicologie, Chimie et Imageries PhD school (MTCI, ED 563), Université Paris Cité.

Conflict of interest

The authors declare no conflict of interest.

Author contributions

GK, DL and HML conceptualized and designed experiments. AG and GK performed generation of mutants and plasmids. AG, GK and NA conducted

BACTH assays. AG, GK, QGG and POV analysed corresponding data. JD conducted nucleotide quantification. AG and JD analysed corresponding data. AG and NA performed bacterial growth experiments and competition assays. SVG synthesized the AIR compound. AG and NA expressed, purified and conducted enzymatic assays for PurK variants. AG, DL and HML wrote the draft of the manuscript. All authors edited the paper.

Peer review

The peer review history for this article is available at <https://publons.com/publon/10.1111/febs.16746>.

Data availability statement

All other data and inquiries are available from HML upon request.

References

- 1 Srere PA (1985) The metabolon. *Trends Biochem Sci* **10**, 109–110.
- 2 Castellana M, Wilson MZ, Xu YF, Joshi P, Cristea IM, Rabinowitz JD, Gitai Z & Wingreen NS (2014) Enzyme clustering accelerates processing of intermediates through metabolic channeling. *Nat Biotechnol* **32**, 1011–1018.
- 3 Meyer FM, Gerwig J, Hammer E, Herzberg C, Commichau FM, Volker U & Stulke J (2011) Physical interactions between tricarboxylic acid cycle enzymes in *Bacillus subtilis*: evidence for a metabolon. *Metab Eng* **13**, 18–27.
- 4 Zhang Y, Beard KFM, Swart C, Bergmann S, Krahnert I, Nikoloski Z, Graf A, Ratcliffe RG, Sweetlove LJ, Fernie AR *et al.* (2017) Protein-protein interactions and metabolite channelling in the plant tricarboxylic acid cycle. *Nat Commun* **8**, 15212.
- 5 Campanella ME, Chu H & Low PS (2005) Assembly and regulation of a glycolytic enzyme complex on the human erythrocyte membrane. *Proc Natl Acad Sci USA* **102**, 2402–2407.
- 6 Dutow P, Schmidl SR, Ridderbusch M & Stulke J (2010) Interactions between glycolytic enzymes of *Mycoplasma pneumoniae*. *J Mol Microbiol Biotechnol* **19**, 134–139.
- 7 Jin M, Fuller GG, Han T, Yao Y, Alessi AF, Freeberg MA, Roach NP, Moresco JJ, Karnovsky A, Baba M *et al.* (2017) Glycolytic enzymes coalesce in G bodies under hypoxic stress. *Cell Rep* **20**, 895–908.
- 8 Kohnhorst CL, Kyoung M, Jeon M, Schmitt DL, Kennedy EL, Ramirez J, Bracey SM, Luu BT, Russell SJ & An S (2017) Identification of a multienzyme complex for glucose metabolism in living cells. *J Biol Chem* **292**, 9191–9203.
- 9 Nielsen KA, Tattersall DB, Jones PR & Moller BL (2008) Metabolon formation in dhurrin biosynthesis. *Phytochemistry* **69**, 88–98.
- 10 Stark M, Raz S & Assaraf YG (2021) Folylpoly- γ -glutamate synthetase association to the cytoskeleton: implications to folate metabolon compartmentalization. *J Proteomics* **239**, 104169.
- 11 Islam MM, Nautiyal M, Wynn RM, Mobley JA, Chuang DT & Hutson SM (2010) Branched-chain amino acid metabolon: interaction of glutamate dehydrogenase with the mitochondrial branched-chain aminotransferase (BCATm). *J Biol Chem* **285**, 265–276.
- 12 Hajj Chehade M, Pelosi L, Fyfe CD, Loiseau L, Rascalou B, Brugiere S, Kazemzadeh K, Vo CD, Ciccone L, Aussel L *et al.* (2019) A soluble metabolon synthesizes the isoprenoid lipid ubiquinone. *Cell Chem Biol* **26**, 482–492.e7.
- 13 Pareek V, Pedley AM & Benkovic SJ (2020) Human de novo purine biosynthesis. *Crit Rev Biochem Mol Biol* **56**, 1–16.
- 14 Pedley AM & Benkovic SJ (2017) A new view into the regulation of purine metabolism: the Purinosome. *Trends Biochem Sci* **42**, 141–154.
- 15 An S, Kumar R, Sheets ED & Benkovic SJ (2008) Reversible compartmentalization of *de novo* purine biosynthetic complexes in living cells. *Science* **320**, 103–106.
- 16 Pareek V, Sha Z, He J, Wingreen NS & Benkovic SJ (2021) Metabolic channeling: predictions, deductions, and evidence. *Mol Cell* **81**, 3775–3785.
- 17 Chua SM & Fraser JA (2020) Surveying purine biosynthesis across the domains of life unveils promising drug targets in pathogens. *Immunol Cell Biol* **98**, 819–831.
- 18 Buchanan JM & Hartman SC (1959) Enzymic reaction in the synthesis of the purines. *Adv Enzymol Relat Areas Mol Biol* **21**, 199–261.
- 19 Zhang Y, Morar M & Ealick SE (2008) Structural biology of the purine biosynthetic pathway. *Cell Mol Life Sci* **65**, 3699–3724.
- 20 Zhao H, Chiaro CR, Zhang L, Smith PB, Chan CY, Pedley AM, Pugh RJ, French JB, Patterson AD & Benkovic SJ (2015) Quantitative analysis of purine nucleotides indicates that purinosomes increase de novo purine biosynthesis. *J Biol Chem* **290**, 6705–6713.
- 21 Chan CY, Zhao H, Pugh RJ, Pedley AM, French J, Jones SA, Zhuang X, Jinnah H, Huang TJ & Benkovic SJ (2015) Purinosome formation as a function of the cell cycle. *Proc Natl Acad Sci USA* **112**, 1368–1373.
- 22 Doigneaux C, Pedley AM, Mistry IN, Papayova M, Benkovic SJ & Tavassoli A (2020) Hypoxia drives the assembly of the multienzyme purinosome complex. *J Biol Chem* **295**, 9551–9566.

- 49 Karimova G, Davi M & Ladant D (2012) The beta-lactam resistance protein Blr, a small membrane polypeptide, is a component of the *Escherichia coli* cell division machinery. *J Bacteriol* **194**, 5576–5588.
- 50 Shannon P, Markiel A, Ozier O, Baliga NS, Wang JT, Ramage D, Amin N, Schwikowski B & Ideker T (2003) Cytoscape: a software environment for integrated models of biomolecular interaction networks. *Genome Res* **13**, 2498–2504.
- 51 Munier H, Gilles A-M, Glaser P, Krin E, Danchin A, Sarfati R & Barzu O (1991) Isolation and characterization of catalytic and calmodulin-binding domains of *Bordetella pertussis* adenylate cyclase. *Eur J Biochem* **196**, 469–474.
- 52 BD Biosciences (2003) BD TALON metal affinity resins user manual. BD Biosciences.
- 53 Walker JM (2005) The proteomics protocols handbook. Humana, Totowa, NJ.
- 54 Srivastava PC, Mancuso RW, Rousseau RJ & Robins RK (1974) Nucleoside peptides. 6. Synthesis of certain N-(5-amino-1-(beta-D-ribofuranosyl)imidazole-4-carbonyl)amino acids related to naturally occurring intermediates in the purine biosynthetic pathway. *J Med Chem* **17**, 1207–1211.
- 55 Groziak MP, Bhat B & Leonard NJ (1988) Nonenzymatic synthesis of 5-aminoimidazole ribonucleoside and recognition of its facile rearrangement. *Proc Natl Acad Sci USA* **85**, 7174–7176.
- 56 Dautin N, Karimova G, Ullmann A & Ladant D (2000) Sensitive genetic screen for protease activity based on a cyclic AMP signaling cascade in *Escherichia coli*. *J Bacteriol* **182**, 7060–7066.
- 57 Karimova G, Dautin N & Ladant D (2005) Interaction network among *Escherichia coli* membrane proteins involved in cell division as revealed by bacterial two-hybrid analysis. *J Bacteriol* **187**, 2233–2243.
- 58 Larkin MA, Blackshields G, Brown NP, Chenna R, McGettigan PA, McWilliam H, Valentin F, Wallace IM, Wilm A, Lopez R *et al.* (2007) Clustal W and Clustal X version 2.0. *Bioinformatics* **23**, 2947–2948.
- 59 Robert X & Gouet P (2014) Deciphering key features in protein structures with the new ENDscript server. *Nucleic Acids Res* **42**, W320–W324.
- 60 Holmes EW, McDonald JA, McCord JM, Wyngaarden J & B., & Kelley, W. N. (1973) Human glutamine phosphoribosylpyrophosphate amidotransferase: kinetic and regulatory properties. *J Biol Chem* **248**, 144–150.
- 61 Messenger LJ & Zalkin H (1979) Glutamine phosphoribosylpyrophosphate amidotransferase from *Escherichia coli* purification and properties. *J Biol Chem* **254**, 3382–3392.
- 62 Cheng YS, Rudolph J, Stern M, Stubbe J, Flannigan KA & Smith JM (1990) Glycinamide ribonucleotide synthetase from *Escherichia coli*: cloning, overproduction, sequencing, isolation, and characterization. *Biochemistry* **29**, 218–227.
- 63 Welin M, Grossmann JG, Flodin S, Nyman T, Stenmark P, Trésaugues L, Kotenyova T, Johansson I, Nordlund P & Lehtiö L (2010) Structural studies of tri-functional human GART. *Nucleic Acids Res* **38**, 7308–7319.
- 64 Inglese J, Johnson DL, Shiao A, Smith JM & Benkovic SJ (1990) Subcloning, characterization, and affinity labeling of *Escherichia coli* glycinamide ribonucleotide transformylase. *Biochemistry* **29**, 1436–1443.
- 65 Marolewski A, Smith JM & Benkovic SJ (1994) Cloning and characterization of a new purine biosynthetic enzyme: a non-folate glycinamide ribonucleotide transformylase from *E. coli*. *Biochemistry* **33**, 2531–2537.
- 66 Thoden JB, Firestine S, Nixon A, Benkovic SJ & Holden HM (2000) Molecular structure of *Escherichia coli* PurT-encoded glycinamide ribonucleotide Transformylase. *Biochemistry* **39**, 8791–8802.
- 67 Barnes TS, Bleskan JH, Hart IM, Walton KA, Barton JW & Patterson D (1994) Purification of, generation of monoclonal antibodies to, and mapping of phosphoribosyl N-formylglycinamide amidotransferase. *Biochemistry* **33**, 1850–1860.
- 68 Schendel FJ, Mueller E & Stubbe J (1989) Formylglycinamide ribonucleotide synthetase from *Escherichia coli*: cloning, sequencing, overproduction, isolation and characterization. *Biochemistry* **28**, 2459–2471.
- 69 Schrimsher JL, Schendel FJ & Stubbe J (1986) Purification and characterization of aminoimidazole ribonucleotide synthetase from *Escherichia coli*. *Biochemistry* **25**, 4366–4371.
- 70 Li S-X, Tong Y-P, Xie X-C, Wang Q-H, Zhou H-N, Han Y, Zhang Z-Y, Gao W, Li S-G, Zhang XC *et al.* (2007) Octameric structure of the human bifunctional enzyme PAICS in purine biosynthesis. *J Mol Biol* **366**, 1603–1614.
- 71 Green SM, Malik T, Giles IG & Drabble WT (1996) The purB gene of *Escherichia coli* K-12 is located in an operon. *Microbiology* **142** (Pt. 11), 3219–3230.
- 72 Lee P & Colman RF (2007) Expression, purification, and characterization of stable, recombinant human adenylosuccinate lyase. *Protein Expr Purif* **51**, 227–234.
- 73 Rayl EA, Moroson BA & Beardsley GP (1996) The human purH gene product, 5-aminoimidazole-4-carboxamide ribonucleotide formyltransferase/IMP cyclohydrolase: cloning, sequencing, expression, purification, kinetic analysis, and domain mapping. *J Biol Chem* **271**, 2225–2233.
- 74 Carr SF, Papp E, Wu JC & Natsumeda Y (1993) Characterization of human type I and type II IMP dehydrogenases. *J Biol Chem* **268**, 27286–27290.

- 75 Labesse G, Alexandre T, Vaupré L, Salard-Arnaud I, Him JLK, Raynal B, Bron P & Munier-Lehmann H (2013) MgATP regulates Allostery and fiber formation in IMPDHs. *Structure* **21**, 975–985.
- 76 Powell G, Rajagopalan KV & Handler P (1969) Purification and properties of Inosinic acid dehydrogenase from *Escherichia coli*. *J Biol Chem* **244**, 4793–4797.
- 77 Nakamura J & Lou L (1995) Biochemical characterization of human GMP synthetase. *J Biol Chem* **270**, 7347–7353.
- 78 Sakamoto N, Hatfield GW & Moyed HS (1972) Physical properties and subunit structure of xanthosine 5'-phosphate aminase. *J Biol Chem* **247**, 5880–5887.
- 79 Bass MB, Fromm HJ & Stayton MM (1987) Overproduction, purification, and characterization of adenylosuccinate synthetase from *Escherichia coli*. *Arch Biochem Biophys* **256**, 335–342.
- 80 Sampaleanu LM, Yu B & Howell PL (2002) Mutational analysis of duck delta 2 crystallin and the structure of an inactive mutant with bound substrate provide insight into the enzymatic mechanism of argininosuccinate lyase. *J Biol Chem* **277**, 4166–4175.
- 81 Wang W, Gorrell A, Honzatko RB & Fromm HJ (1997) A study of *Escherichia coli* adenylosuccinate synthetase association states and the interface residues of the homodimer. *J Biol Chem* **272**, 7078–7084.